11

Measurement of Strain Distribution of Composite Materials by Electron Moiré Method

Satoshi Kishimoto, Yoshihisa Tanaka,
Kimiyoshi Naito and Yutaka Kagawa
National Institute for Materials Science
Japan

1. Introduction

It is very important to measure the local strain and stress distributions for understanding the mechanical properties of structural materials. Therefore, there are many techniques to measure the strain or stress distribution such as the strain gage method, optical elasticity method, optical Moiré method, etc. In these methods, the optical Moiré method (Weller & Shepard, 1948; Morse et al., 1960; Sciammarela & Durelli, 1961; Durelli & Parks, 1970; Theocaris, 1969; Post et al, 1994; Chiang, 1982; Post, 1988) is one of the convenient methods to measure the deformation of the materials. However, these methods are difficult to apply for deformation measurements from a microscopic aspect.

To measure the micro-deformation in a very small area, the authors have developed an electron Moiré method (Kishimoto et al., 1991, 1993) , and J.W. Dally, D. T. Read (Read & Dally, 1994; Dally &.Read, 1993) and H. Xie (Xie et al., 2007) advocated it. This method keeps the main advantages of the moiré and laser moiré interferometry methods, and has the additional ability of measuring deformation in a micro-area with a high sensitivity. Besides, the electron moiré method also uses a wide range for measuring the deformation. The range of the measurable deformation is from 25microns to 0.1micron using a model grid with different pitches.

To measure the micro-deformation i.e. sliding and slip lines in a smaller area, micro-grid method is very useful. Compare these two methods, electron moiré method is easy to understand the strain distribution and the large sliding (Kishimoto et al., 1991, 1993).

In this study, In order to pursue the application of the electron moiré method, some typical experiments were performed. The strain distribution at the interface of the laminated steel, strain distribution of the fiber and the matrix in the fiber reinforced plastic, the thermal strain in or around the metallic fiber in Al alloy were observed.

2. Experimental procedure

2.1 The principle of the electron Moiré method

The principle of the optical moiré method is shown in Figure 1 (a). In this method, moiré fringes can be observed when two gird (model grid and master grid) are overlapped. From

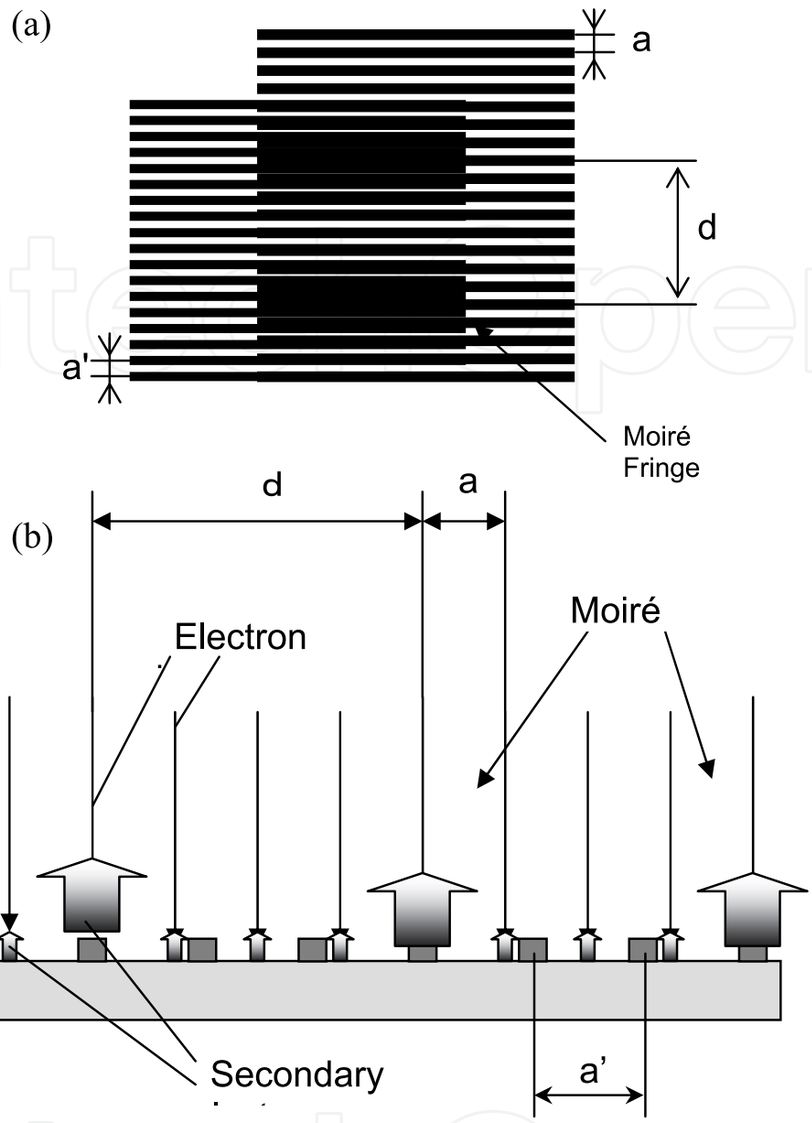

Fig. 1. Schematic formation of moiré fringe; (a) and the spacing of master grid ;(b) electrons after secondary.

the spacing of moiré fringes, and the spacing of master grid, the strain can be calculated. A principle of an electron moiré method is shown in Figure 1 (b) and as follows. A model grid is prepared on the surface of the specimen before deformation by using electron beam lithography or photo-lithography. Before and after deformation, the specimen is mounted on the specimen stage in a scanning electron microscope (SEM) and an electron beam scan having spaces almost same as that of the model grid can be used for the master-grid. The difference in the amount of the secondary electrons per a primary electron makes the Moiré fringes (electron Moiré fringes) that consists bright and dark parts.

2.2 Micro grid fabrication by electron beam lithograph

The procedure for producing a model by using the electron beam lithography (Kishimoto, et. al, 1993) is shown in Figure 2. The specimen must first be polished to a mirror-like finish

(up to 0.05μm Al_2O_3 powder), then it is covered with an electron-sensitive layer (electron beam resist, Nippon Zeon ZEP-520-22 and Toray EBR-9), spinning at a speed of 2,500 RPM for 120 seconds, and then baked in an oven for 30 minutes at 453 K for ZEP-520 and spinning at a speed of 2,000 RPM for 120 seconds, and then baked in an oven for 30 minutes at 468 K for EBR-9.

The specimen was then mounted on the specimen stage in a TOPCON SX-40A SEM for the electron beam exposure. After electron beam exposure, the specimen coated by ZEP-520 was developed in a solution of ZED-N50 for 60 seconds, and then immediately rinsed in ZMD-B for 30 seconds. The specimen coated by EBR-9 was developed in a solution of Type 1 for EBR-9 for 60 seconds, and then immediately rinsed in 2-propanol for 30 seconds. The specimen was coated with a very thin layer (10-20 nm) of gold by plasma sputtering.

The difference in the emitted amount of the secondary electrons per a primary electron between the surface and the deposited layer must be large enough to get produce a contrast in the electron moiré fringe. After removing the resist using an organic solvent, a model grid is formed on the specimen surface.

2.3 Observation of electron moiré fringe and micro-grid

The specimen with micro-grid (model grid) was mounted on the specimen stage in a TOPCON SX-40A SEM for the observation of electron moiré fringe and TOPCON SM-510 for observation of micro-grid. The large difference in the emitted amount of the secondary electrons per a primary electron between the surface and the deposited layer makes it possible observes the micro-grids and the electron moiré fringes.

2.4 Three-point bending test of fiber reinforced plastic

Figure 3 (a) shows a schematic set-up of the three-point bending test specimens. A model grid was prepared near the bottom surface of the carbon fiber reinforced plastic (CFRP) as shown in Figure 2 (b) and a higher magnification SEM image is shown in Figure 3 (c). The strain of the bottom surface (bending strain) was measured by a strain gage. The specimen's surface was observed by an optical microscope (NIKON Opti-Photo) with a CCD camera, and the electron moiré fringes were observed by the scanning electron microscope (TOPCON SX-40A) equipped with a beam blanker and a pattern generator. The specimen was set on the stage of SEM (TOPCON SM-510) with bending devices. SEM images and electron moiré fringes were observed during bending.

2.5 Compression test of laminated steel

Eight sheets of austenite stainless steel (304 stainless steel sheets (SUS304)) of 10-mm thickness and 7 sheets of martensite steel (WT-780C) sheets of 12-mm thickness were alternately overlapped and rolled to 12.7mm at 1473 K after a 2h hold at the same temperature. The thickness of each layer was about from 0.7 mm to 0.9mm.

This laminated steel was cut and machined into specimens with a 10-mm width, 10-mm length and 12-mm height, and then the laminated sides were then polished. On the polished surface, some model grids with a cross grid of 2.9-μm spacing were prepared by electron beam lithography. The compressive tests were performed using a universal tensile test machine (Shimadzu AUTOGRAPH AG-100kND) at room temperature. The loading direction was perpendicular and parallel to the each layer. After the test, the nominal strain

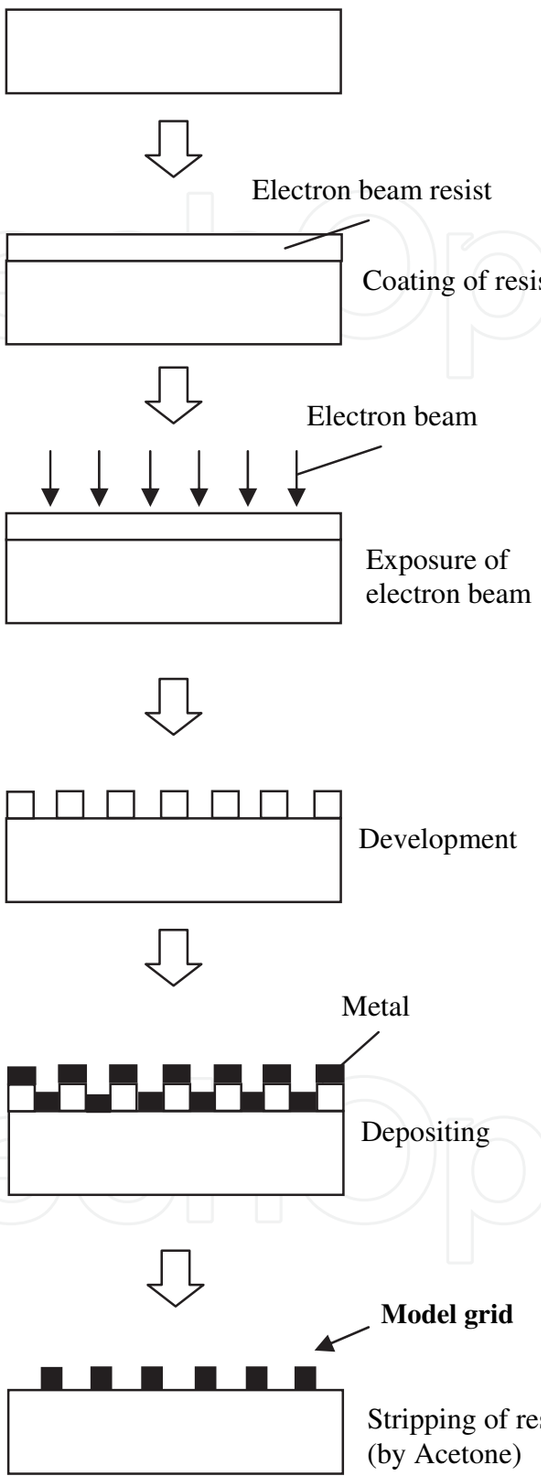

Fig. 2. Schematic image of model grid fabrication process by electron beam lithography.

was measured. The specimen was then placed on the stage of a scanning electron microscope (SEM), and the electron moiré fringe was observed by the electron moiré method. Figures 4 (a) and (b) show the schematic image of compression test specimen and model grid on the specimen's surface, respectively.

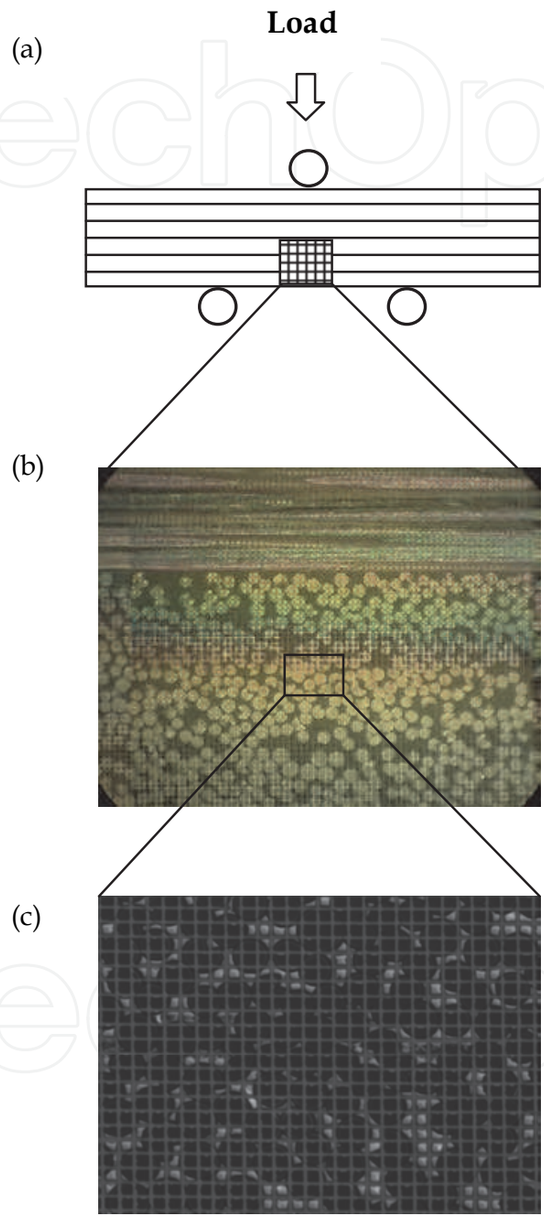

Fig. 3. Schematic image of setup of tree point bending test ;(a) , Optical microscope image on model grid; (b) and SEM image of model grid (spacing of the model grid is 5μm); (c).

2.6 Deformation by thermal expansion

The specimen was made of commercial aluminum alloy with Ti-Ni fibers. The diameter of the Ti-Ni fiber was about 600μm. A sample was cut from the bulk laminates perpendicular

to one fiber axis using a diamond saw, and then polished into a film about 300μm thick. The specimen was put on the heating stage in SEM. The electron moiré fringes before and after heating (up to 353K) were observed. From these moiré fringes, strain change by thermal expansion was calculated and thermal expansion ratio was calculated.

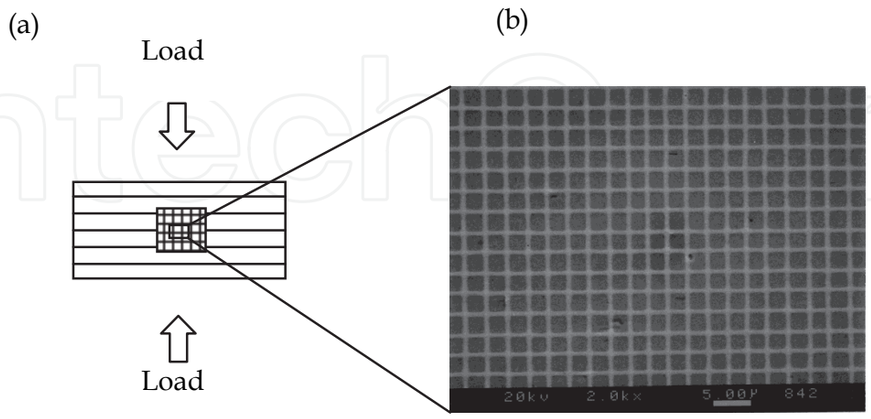

Fig. 4. Schematic image of setup of compression test ;(a) and SEM image of model grid; (b).

3. Result and discussion

3.1 Model grid and electron moiré fringe

Figure 3 (c) and Figure 4 (b) show the model grid fabricated by electron beam lithography. The specimen's surface was observed by a scanning electron microscope (SEM:TOPCON, SM-510), and the electron moiré fringes were observed by the SEM (TOPCON SX-40A) equipped with a beam blanker and a pattern generator. Figure 5 shows the electron moiré fringe created by the electron beam exposure with 3.3 μm spacing onto the model grid (2.9-μm spacing) of the specimen shown in Figure 4 (b).

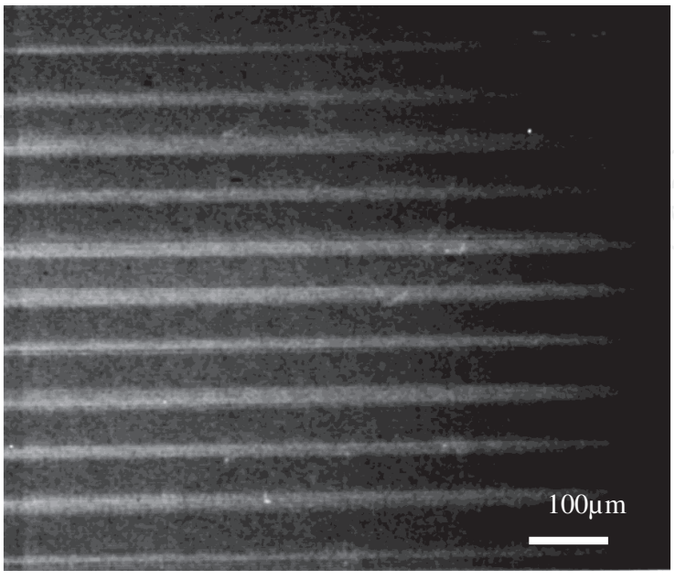

Fig. 5. Electron moiré fringe on the model grid of Figure 4 (b).

3.2 Strain distribution of fiber reinforced plastic under three-point bending test

The strain distribution of a carbon fiber reinforced plastic during a bending test and after initiation of cracks was measured. Figures 6(a) and (c) show SEM images of a same micro-grid on the FRP specimen during bending (maximum strain is 0.1%) and after initiation of cracks (see Figure 7), respectively. Figures 6 (b) and (d) show electron Moiré fringes of the same place during bending (maximum strain is 0.1%) and after initiation of cracks, respectively. The electron beam exposure with a 4.5μm spacing onto the model grid (5 μm spacing) of the specimen creates the electron moiré fringes. Figure 6 (b) and (d) show electron Moiré fringe fabricated by electron beam scan in the horizontal direction. Strain distribution in the horizontal direction, ε_x is also indicated in this figures. Strain ε_x can be calculated by using the images of the electron Moiré fringes and eq. (1). Using the moiré patterns, the strain ε can be calculated, which are expressed as follows, (Kishimoto et al., 1991, 1993)

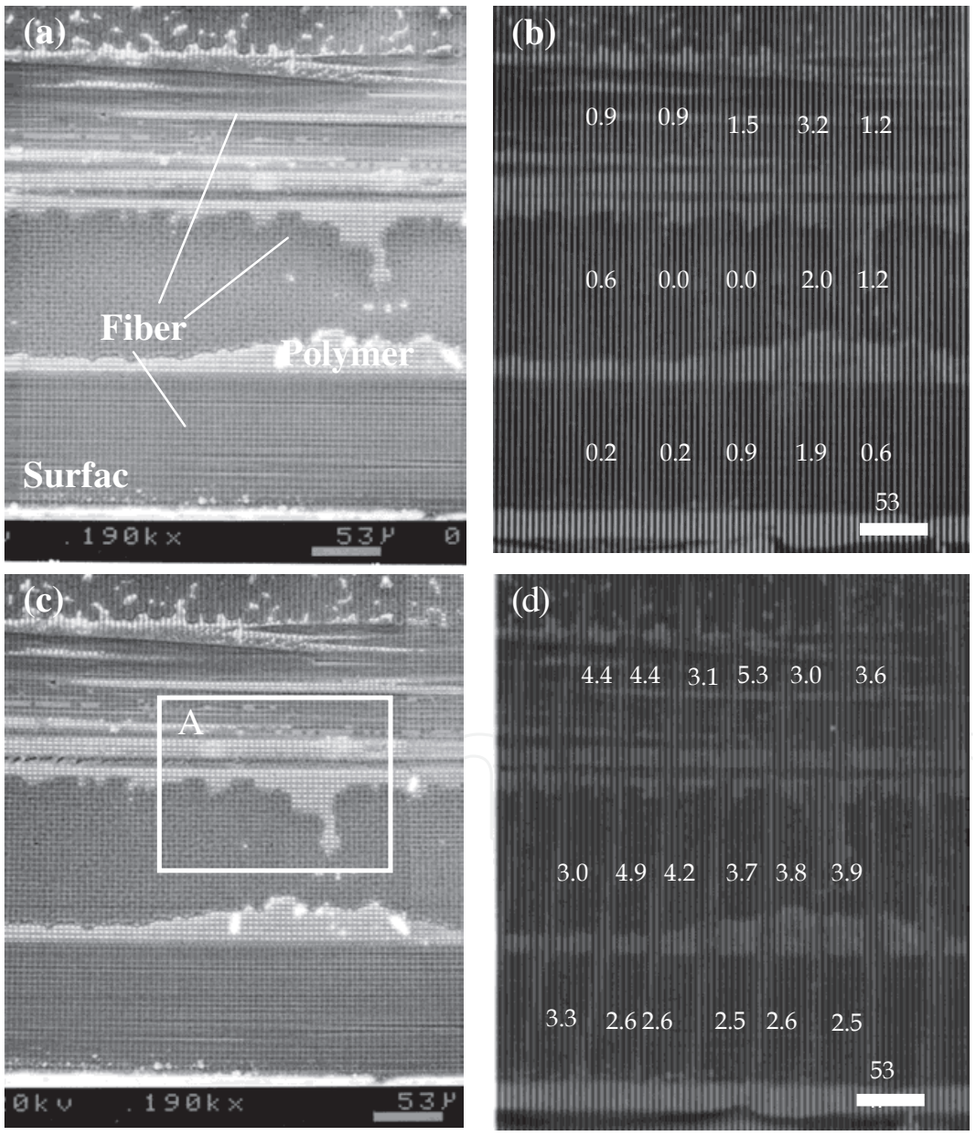

Fig. 6. SEM image; (a) and electron moiré fringe; (b) at 0.1% maximum strain and SEM image; (c) and electron moiré fringe; (d) after cracking of FRP specimen.

$$e = a/(d-a)-(a'-a)/a \quad (1)$$

where, **d**, **a** and **a'** are the spacing of the Moiré fringe, the spacing of the electron beam scan and the spacing of the model grid before deformation, respectively. The strain in a 100μm area can be measured using the electron Moiré method. Before initiation of the cracks, the strain ε_x is tensile and almost same. However, after initiation of the cracks, strain ε_x near the surface and inside is different. The strain ε_x near the surface is smaller than that of inside. It should be thought that stress near the surface of the specimen was released by the cracking.

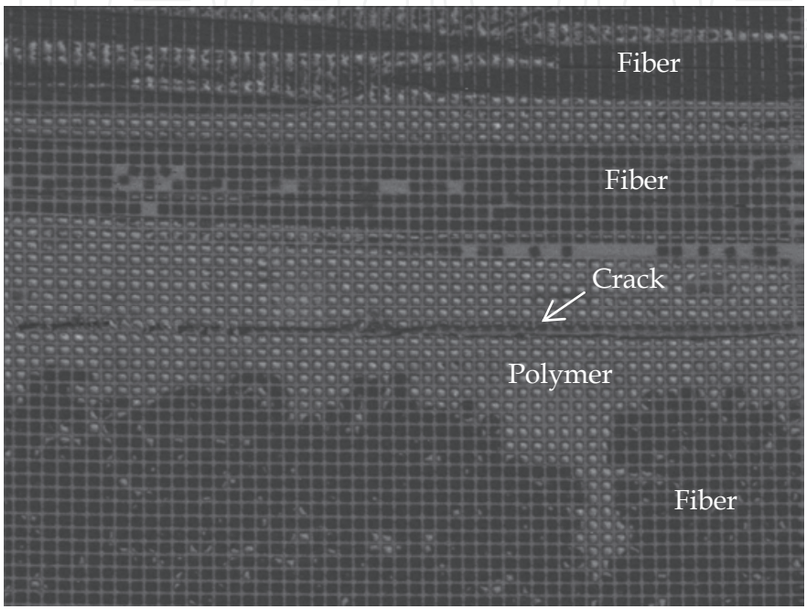

Fig. 7. Higher magnification SEM images of the area A in Figure 6 (c).

3.3 Compressive deformation of laminated steel

The strain distribution of laminated steel after a compression test (about -4.6%) was measured. igures 8 (a) and (d) show SEM images of the micro-grid area, Figures 8 (b), (c), (e) and (f) show an example of the electron Moiré fringe after the compression test. For Figure 8 (a), (b) and (c), the loading direction is perpendicular to the laminate sheets and for Figure 8 (d), (e) and (f), the loading direction is parallel to the laminate sheets. These electron moiré fringes are created by electron beam exposure with 3.3-μm spacing onto the model grid (2.9-μm spacing) of the specimen (Figures 8 (b) and (e)) and electron beam exposure with 2.5-μm spacing onto the model grid (3.2-μm spacing) of the specimen (Figures 8 (c) and (f)). Also, the electron moiré fringes in Figures 8 (b) and (e) is formed by the electron beam scan in the direction perpendicular to the loading direction and the electron moiré fringes in (Figures 8 (c) and (f) is formed by the electron beam scan in the loading direction. The boundaries between SUS304 and WT-780, the parts of SUS304 and WT-780 and the bottom surface are also shown in the same figures.

In Figure 8 (b), (c), (e) and (f), the electron beam moiré fringes are complicated. In Figure 8 (b), (c), (e) and (f), the shape of the electron moiré fringe is wavy and the spacing of moiré fringe is different in places. This means that the strain in the horizontal direction, ε_x and the strain in the vertical direction, εy is different at each point and distributed largely. Near the boundary between WT-780C and SUS304, the strain ε_y is larger than that of other places.

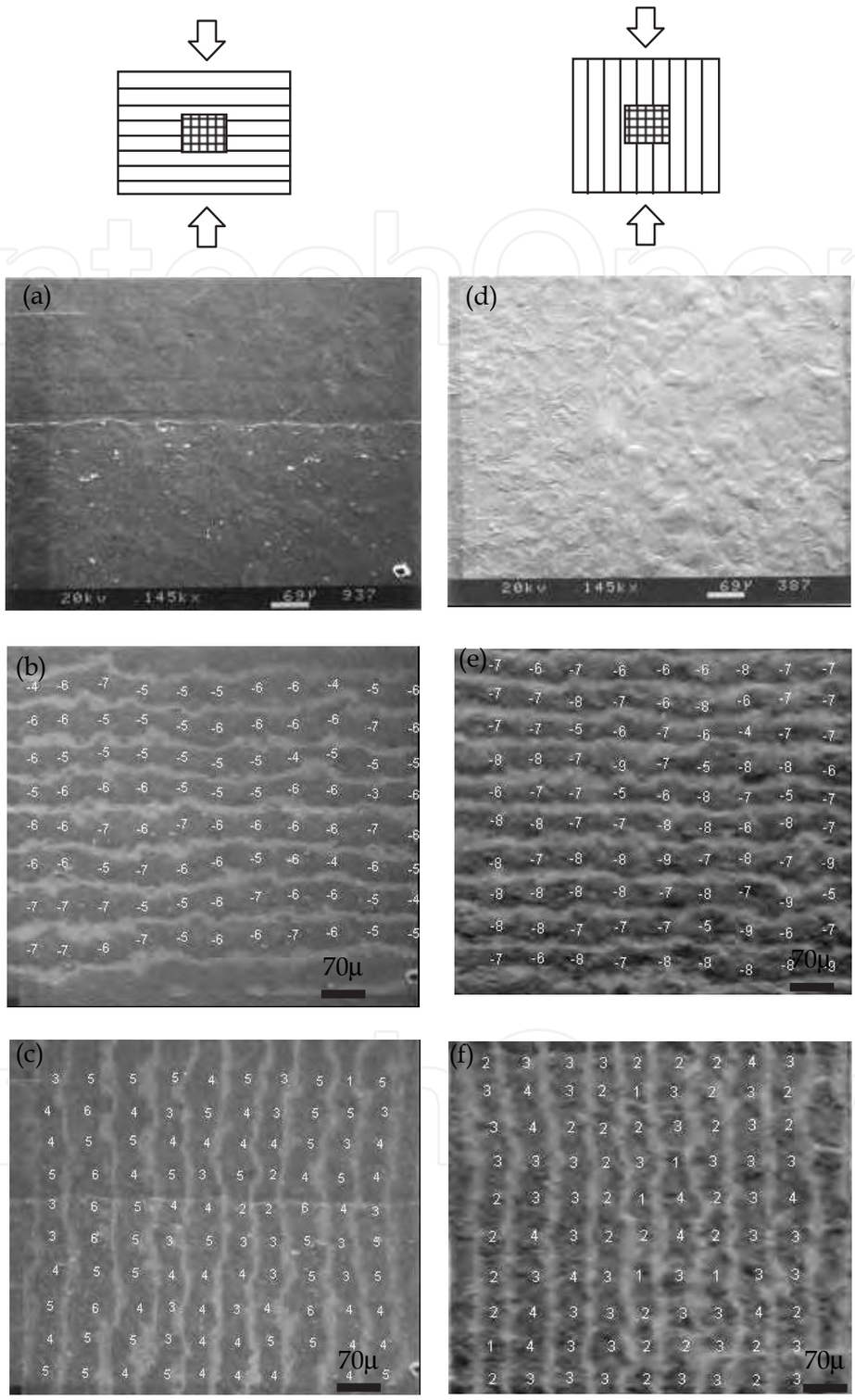

Fig. 8. SEM images; (a) and (b), electron moiré fringe in the direction perpendicular to the loading axis; (c) and (d), and electron moiré fringe in the loading direction; (e) and (f)after about 4.5% compressive deformation. **(**Numbers are distributed strain (%) at same point)

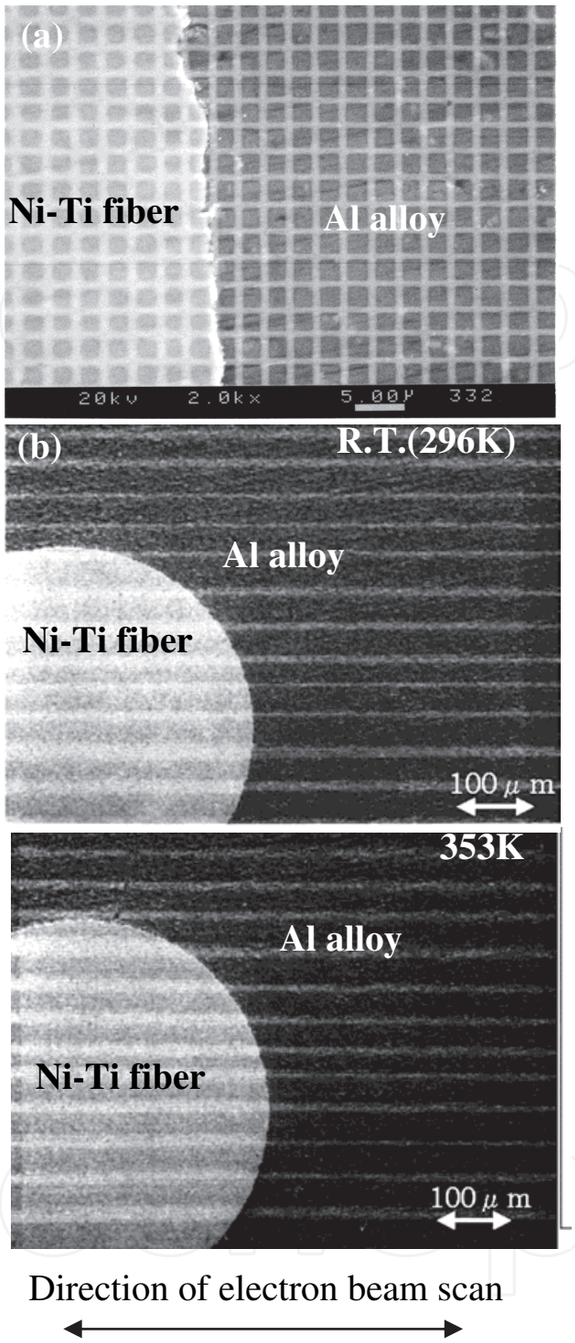

Fig. 9. Higher magnification SEM image of model grid; (a), electron moiré fringes around the Ti-Ni fibers in Al alloy at room temperature; (b) and electron moiré fringes around the Ti-Ni fibers in Al alloy at room temperature at 353K; (c).

The strains in Figure 8 (b) and (c), ε_x, and ε_y, changed from +1% to +6% and -3% to -7%, respectively. The strains in Figure 8 (e) and (f), ε_x, and ε_y, changed from +1% to +4% and -5% to -9%, Compare with the strains ε_x, and ε_y, in the SUS304 area and WT-780C area absolute value of ε_x, and ε_y, is almost same. However, the strain was distributed largely.

3.4 Deformation by thermal expansion

Al alloy with Ni-Ti fiber which had a model grid was set on the heating stage in an SEM chamber and the electron moiré fringes before and after heating were observed. Figure 9 (a), (b) and (c) show an SEM image of the morel grid with 2.9 μm spacing, electron moiré fringes before (room temperature (296K)) and after heating (353K), respectively. Electron beam exposure of 2.7 μm spacing Strain on to the model grid (2.9 μm spacing) on the specimen's surface created the electron moiré fringe.

Strain caused by thermal expansion was calculated by using equation (1). The strain of the Ni-Ti fiber part and Al alloy part caused by the heating was 0.23% and 0.15%, respectively. From these values, coefficient of thermal expansion was also calculated. The coefficient of thermal expansion of the Ni-Ti fiber and Al alloy in this material was 4.0×10^{-5}/K and 2.6×10^{-5}/K, respectively.

4. Conclusion

The strain distribution of the fiber and the matrix in the fiber reinforced plastic, around the interface of the laminated steel, the thermal strain in or around the metallic fiber in Al alloy were observed by electron moiré method. After initiation of cracksi FRP non-uniform deformation was observed. Non-uniform deformation near the boundary of laminated steel of brittle martensitic steel (WT-780) and ductile austenite stainless steel (SUS304) during compressive test was observed. Also, thermal expansion could be observed and coefficient of thermal expansion was calculated.

5. Acknowledgment

This work was partly supported by the LISM (Layer-Integrated Steel and Metal) Project by the Ministry of Education, Culture, Sports, Science and Technology (MEXT), Japan and the Failsafe hybrid composite project of the National Institute for Materials Science, Japan.

6. References

Weller, R and Shepard, B.M., (1948) Displacement measurement by mechanical interferometry, *Proc. Soc. for Exp. Stress Anal.*, 6 35–38

Morse, S.A., Durelli, J., and Sciammarella, C.A., (1960),Geometry of moiré fringes in strain analysis, *J. Eng. Mech. Div.,* 86 105-126.

Sciammarela, C.A., Durelli, A.J, (1961) Moiré fringes as a means of analyzing strains, *J. Eng. Mech. Div.,* 87, 55-74.

Durelli, A.J., Parks, V.J., Moiré, (1970) Analysis of Strain, Prentice Hall..

Theocaris, S., (1969) Moiré Fringe in Strain Analysis, Pergamon..

Post, D. , Han B., Ifju, P., (1994) High Sensitivity Moiré, Springer.

Chiang, F.P., (1982), Moiré method of strain analysis Manual on Experimental Stress Analysis 5th edn, Doyle and Phillips, Society for Experimental Mechanics, 107–35

Post, D., (1988) Sharping and multiplication of moiré fringe, *Exp. Mech.* 28 329

Kishimoto, S., Egashira, M., Shinya, N.and Carolan, R.A., (1991) Local Micro-deformation Analysis by Means of Micro-grid and Electron beam Moiré Fringe Method, *Proc. 6th Int. Conf. on Mech. Behavior of Materials*, Pargamon Press, pp.661-666,

Kishimoto, S., Egashira, M. and Shinya, N., (1993) Micro-creep deformation measurement by a moiré method using electron beam lithography and electron beam scan, *Opt. Eng.*, 32 522-526 .

Read D.T and Dally, J.W., (1994), Electron Beam Moiré Study of Fracture of a Glass Fiber Reinforced Plastic Composite, *J APPL MECH-T ASME*, 61, 402-409.

Dally, J.W., Read, D.T., (1993), Electron-Beam Moiré, *Exp. Mech.* 33, 270-277.

Read D.T and Dally, J.W., Szanto, M., (1993) Scanning moiré at high magnification using optical methods, *Exp. Mech.*, 33 110

Xie, H., Wang, Q., Kishimoto, S., Dai, F., (2007) Characterization of planar periodic structure using inverse laser scanning confocal microscopy moiré method and its application in the structure of butterfly wing, *J. Applied Physics*, 101, 103511.

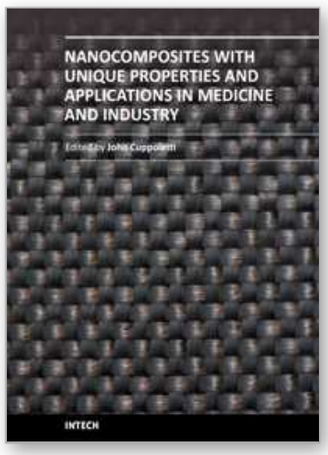

Nanocomposites with Unique Properties and Applications in Medicine and Industry

Edited by Dr. John Cuppoletti

ISBN 978-953-307-351-4
Hard cover, 360 pages
Publisher InTech
Published online 23, August, 2011
Published in print edition August, 2011

This book contains chapters on nanocomposites for engineering hard materials for high performance aircraft, rocket and automobile use, using laser pulses to form metal coatings on glass and quartz, and also tungsten carbide-cobalt nanoparticles using high voltage discharges. A major section of this book is largely devoted to chapters outlining and applying analytic methods needed for studies of nanocomposites. As such, this book will serve as good resource for such analytic methods.

InTech Europe
University Campus STeP Ri
Slavka Krautzeka 83/A
51000 Rijeka, Croatia
Phone: +385 (51) 770 447
Fax: +385 (51) 686 166
www.intechopen.com

InTech China
Unit 405, Office Block, Hotel Equatorial Shanghai
No.65, Yan An Road (West), Shanghai, 200040, China
中国上海市延安西路65号上海国际贵都大饭店办公楼405单元
Phone: +86-21-62489820
Fax: +86-21-62489821

IntechOpen